Classification and Discretization of Shadowing Toward Low Storage Radio Map

Keita Katagiri† and Takeo Fujii†
† Advanced Wireless and Communication Research Center (AWCC), The University of Electro-Communications
1–5–1 Chofugaoka, Chofu, Tokyo 182–8585, Japan
Email: {katagiri, fujii}@awcc.uec.ac.jp

***Abstract*—This paper considers the shadowing classifier and shadowing discretization to create a low storage radio map. We have confirmed that the data size of the radio map can be reduced while high estimation accuracy keeps via the former method. However, the data size has not been evaluated using the latter method that simply discretizes a shadowing realization in each position. Thus, this paper discusses the effectiveness of the two methods in terms of the data size and estimation accuracy. The verification results show that the shadowing classifier can skillfully predict the radio propagation compared with the discretization-based method. Meanwhile, if the slight degradation of the estimation accuracy is tolerated, the discretization-based method may be useful.**

***Index Terms*—Radio map, classification, radio propagation, discretization**

I. Introduction

Several researchers are studying a radio map as a tool to skillfully grasp the radio propagation [1], [2]. The radio map often visualizes the average received signal power in each reception position by processing measured datasets collected by mobile terminals. The created radio map is stored as the statistical data in a cloud server and is provided to a transmitter and receivers. The site specific radio propagation can be precisely estimated via the radio map.

However, because the conventional radio map stores the average received signal power in each position, the enormous data may be registered according to the communication area range. To reduce the registered data size, it is necessary to unify average received signal power values in a certain area range. However, if this area range is too wide, the average received signal power may be inaccurately calculated owing to the fluctuation of the radio propagation. Obviously, there is the trade-off between the estimation accuracy and the area range for which the average power is derived.

It is well known that there is empirically the spatial correlation in the shadowing realization [3]. The reference [3] has clarified that the correlation coefficient can be approximately expressed as the exponential decay model in terms of the moving distance. This fact means that the shadowing realizations may be similar in neighborhood position.

Focusing on this property, we have proposed the shadowing classifier [4] to reduce the registered data size of the radio map. This method creates K shadowing realizations by quantizing measured data. Then, a quantized shadowing is assigned to each location according to the proposed objective function that minimize the error between the quantized shadowing and instantaneous received signal power values. We have confirmed that the shadowing classifier can construct the accurate radio map with low registered data size.

However, if the communication area range is wide, the conventional classifier may take the long time to assign a shadowing to each position. This is because the processing load becomes enormous owing to the calculation of the objective function in each position. Here, as a simpler method, we can consider the discretization of the shadowing realization in each position. This method simply discretizes a shadowing based on the rounding without using the objective function. As a result, the registered data size may be reduced with low processing load compared to the shadowing classifier.

This paper discusses the effectiveness of the shadowing discretization in terms of the data size and estimation accuracy. The verification results show that the shadowing classifier can skillfully predict the radio propagation compared with the discretization-based method. Meanwhile, if the slight degradation of the estimation accuracy is tolerated, the discretization-based method may be useful.

The remainder of this paper is organized as follows. Sect. II mentions the conventional radio map and its issue. After that, the shadowing classifier and the discretization are presented in Sects. III and IV. Then, Sect. V explains the comparative methods for the shadowing classification. After the 3.5GHz band datasets are elucidated in Sect. VI, the verification results are described in Sect. VII. Finally, we conclude this paper in Sect. VIII.

II. Conventional Radio Map

The radio map is usually constructed based on an actual observation of radio environment. Mobile devices, such as smartphones, observe radio environment information in each location and upload these data to the cloud server. This paper assumes that the instantaneous received signal power and reception position are observation dataset in each position. The cloud server splits the communication area into a square area called a mesh. Then, the radio map is created by averaging the instantaneous received signal power samples in each mesh. Such the construction method is well known as *crowdsourcing* [5], [6]. Crowdsourcing enables us to efficiently construct a radio map in terms of the short observation time. The most

advantage of the radio map is accurate prediction of the path loss and shadowing based on actual observations.

However, since the conventional radio map accumulates the average received signal power along with a mesh code [7] in each mesh, the enormous data may be stored according to the area size. Thus, this paper focuses on the reduction of the registered data size in the radio map based on the classification of the shadowing realizations.

III. Shadowing Classifier

We have proposed the shadowing classifier [4] to reduce the registered data size of the radio map. This classifier constructs K shadowing realizations by analyzing measured datasets. For the explanation, this paper assumes that there are L meshes $(l = 0, 1, \cdots, L-1)$ in the communication area. The k-th propagation model $(k = 0, 1, \cdots, K-1)$ is given by

$$\bar{P}_k(d_l) = b - 10a\log_{10}(d_l) + \hat{s}_k \quad [\mathrm{dBm}], \tag{1}$$

where $\bar{P}_k(d_l)$ is the average received signal power estimated by the k-th model, d_l [m] denotes the link distance between the transmitter and the l-th mesh, b [dBm] is the constant value that includes the transmission power and antenna effects, a is a path loss index, and $\hat{s}_k$ [dB] is the k-th quantized shadowing realization. The cloud server first generates the scatter diagram as the horizontal axis is $\log_{10}(d_l)$ and the vertical axis is the average received power in each mesh. After that, we can obtain the parameters b and a based on the least squares method. This paper assumes that b and a are constant in all meshes.

A. Quantization of Shadowing

The cloud server first calculates a non-quantized shadowing realization s_l [dB] in the l-th mesh as follows:

$$s_l = \bar{p}_l - \hat{p}(d_l), \tag{2}$$

where $\bar{p}_l$ [dBm] denotes the average received signal power in the l-th mesh and $\hat{p}(d_l) = b - 10a\log_{10}(d_l)$ [dBm] is the median path loss. A non-quantized shadowing is calculated in each mesh and the shadowing vector $\boldsymbol{s} = (s_0, s_1, \cdots, s_{L-1})$ is created.

After that, the cloud server obtains the maximum shadowing $s_{\max} = \max(\boldsymbol{s})$ [dB] and the minimum shadowing $s_{\min} = \min(\boldsymbol{s})$ [dB], and quantizes between $[s_{\min}, s_{\max}]$ by the step size w [dB]. Thus, we can formulate the k-th quantized shadowing realization $\hat{s}_k$ as,

$$\hat{s}_k = s_{\min} + wk \quad [\mathrm{dB}]. \tag{3}$$

By the processing, the shadowing classifier that consists of different K shadowing models can be generated.

B. Model Assignment

The registered data size can be reduced by assigning the same propagation model to multiple meshes where the radio propagation is similar. For the explanation of the model assignment, this subsection assumes that there are n_l measurement samples $\boldsymbol{p} = (p_1, p_2, \cdots, p_{n_l})$ in the l-th mesh. Here, $\boldsymbol{p}$ is the instantaneous received signal power vector and p_i [dBm] $(i = 1, \cdots, n_l)$ denotes the i-th instantaneous value including small-scale fading. In the radio map construction, the deviation of the average received signal power may be removed by using small mesh size. However, the fluctuation of the small-scale fading may remain a little if the number of samples is too small in the mesh. To consider the effect, the cloud server assigns a propagation model $\bar{P}_k$ to the l-th mesh so that the root mean squared error (RMSE) between $\boldsymbol{p}$ and $\bar{P}_k$ is minimized. The shadowing label k is searched based on the following function,

$$k = \underset{k=0,1,\cdots,K-1}{\arg\min} \sqrt{\frac{1}{n_l}\sum_{i=1}^{n_l}(p_i - \bar{P}_k)^2}. \tag{4}$$

The cloud server registers the shadowing label k as an integer in each mesh as illustrated in Fig. 1.

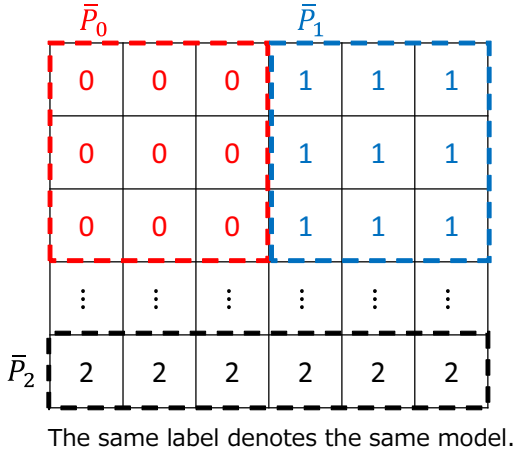

Fig. 1. An overview of the shadowing classification.

IV. Shadowing Discretization

This section explains the second method for reducing the registered data size. The cloud server discretizes the shadowing realization s_l in the l-th mesh by rounding it to the D-th decimal places. This calculation is performed in each mesh and each rounded value is stored in the cloud server. The registration contents of this method will be explained in Sect. VII-C. The average received signal power is derived by considering the median path loss based on b and a in addition to the discretized shadowing.

The same shadowing can be assigned using the small D; however, the estimation accuracy may be slightly degraded owing to the discretization error. Meanwhile, the number of same shadowing models may the small if the large D is used.

V. Comparative Methods

A. Preliminary Descriptions

As the comparative, this paper uses two clustering algorithms: the k-means++ [8] and Gaussian mixture model (GMM). In radio propagation, the shadowing realization has the spatial correlation property that is empirically established as the exponential decay model [3]. Accordingly, similar

shadowing realizations can be observed in vicinity positions. Fortunately, the k-means++ assumes that several data are collectively distributed in a certain area; thus, we use the k-means++ as the first comparison method.

Additionally, the shadowing realization empirically follows the log-normal distribution; that is, this phenomenon matches to the assumed distribution of the GMM. Hence, the GMM is used as the second comparative.

Next, the input data vector is defined as follows:

$$\boldsymbol{z}_l = (x_l, y_l, s_l), \tag{5}$$

where $\boldsymbol{z}_l$ and (x_l, y_l) are the input data vector and the coordinate value in the l-th mesh, respectively. The cloud server calculates (x_l, y_l) based on the mesh code [9].

The coordinate value and shadowing realization are different scales. Therefore, the cloud server standardizes the coordinate value and shadowing realization. Then, a weight is multiplied to each data for changing the impact on the clustering. Note that the standardization is performed using the mean and the standard deviation of each input data.

B. k-means++

k-means++ clusters the input data by minimizing the following evaluation function F:

$$F = \sum_{k=0}^{K-1} \sum_{l=0}^{L-1} u_{lk} d_{\mathrm{e}}(\boldsymbol{z}_l, \boldsymbol{c}_k), \tag{6}$$

where 1 is substituted into u_{lk} if $\boldsymbol{z}_l$ belongs to the k-th cluster; otherwise, 0. $\boldsymbol{c}_k$ denotes the centroid in the k-th cluster and $d_{\mathrm{e}}(\boldsymbol{z}_l, \boldsymbol{c}_k)$ is an euclidean distance between $\boldsymbol{z}_l$ and $\boldsymbol{c}_k$. Here, the number of clusters K corresponds to the number of shadowing models in the proposed classifier.

To determine an initial centroid so that an euclidean distance between each centroid is long, the following procedures are performed:

a). The cloud server randomly picks $\boldsymbol{z}_l$ as the first centroid $\boldsymbol{c}_0$ from the L meshes.

b). The following probability is used to select another centroid $\boldsymbol{c}_k$ from the L meshes, where its input data vector is defined as $\boldsymbol{z}'_l$.

$$\frac{\min\limits_{0 \le k \le K-1} d_{\mathrm{e}}(\boldsymbol{z}'_l, \boldsymbol{c}_k)}{\sum_{l=0}^{L-1} \min\limits_{0 \le j \le K-1} d_{\mathrm{e}}(\boldsymbol{z}_l, \boldsymbol{c}_j)}. \tag{7}$$

c). b). is repeated while K centroids are chosen.

After the selection of the K initial centroids, the shadowing realizations are clustered into K clusters by referring the evaluation function F. Then, the cloud server averages the shadowing realizations having the same cluster label k and registers the averaged value and cluster label k in each mesh.

C. GMM

GMM consists of the linear combinations of several Gaussian distributions. Each input data vector can be clustered by determining a Gaussian distribution that the data belongs to. The k-th probability density function (PDF) of V-variate Gaussian distribution is defined as,

$$\begin{aligned} g_k(\boldsymbol{x}) &= \frac{1}{(2\pi)^{V/2} |\boldsymbol{\Sigma}_k|^{1/2}} \\ &\exp\left(-\frac{1}{2} (\boldsymbol{x} - \boldsymbol{c}_k)^{\mathrm{T}} \boldsymbol{\Sigma}_k^{-1} (\boldsymbol{x} - \boldsymbol{c}_k) \right), \end{aligned} \tag{8}$$

where $\boldsymbol{c}_k$ is the mean vector of the k-th distribution that corresponds to the centroid in the k-means++. Σ_k is the covariance matrix of the k-th distribution. $\boldsymbol{x} = (x_1, \cdots, x_V)$ is the random variable vector and $\boldsymbol{\theta}_k = (\boldsymbol{c}_k, \boldsymbol{\Sigma}_k)$. The PDF of GMM is represented as follows:

$$g(\boldsymbol{x}|\boldsymbol{\Theta}) = \sum_{k=0}^{K-1} \alpha_k g_k(\boldsymbol{x}|\boldsymbol{\theta}_k), \tag{9}$$

where α_k is defined as a mixing coefficient of the k-th distribution and $\boldsymbol{\Theta} = (\alpha_0, \alpha_1, \cdots, \alpha_{K-1}, \boldsymbol{\theta}_0, \boldsymbol{\theta}_1, \cdots, \boldsymbol{\theta}_{K-1})$. Then, the log-likelihood function of GMM is given by

$$\begin{aligned} \log g(\boldsymbol{X}|\boldsymbol{\Theta}) &= \log \prod_{i=1}^{N} g(\boldsymbol{x}_i|\boldsymbol{\Theta}) \\ &= \sum_{i=1}^{N} \log \sum_{k=0}^{K-1} \alpha_k g_k(\boldsymbol{x}_i|\boldsymbol{\theta}_k), \end{aligned} \tag{10}$$

where $\boldsymbol{X} = \{\boldsymbol{x}_1, \boldsymbol{x}_2, ..., \boldsymbol{x}_N\}$ and N is the number of data.

To maximize the log-likelihood function, Expectation-Maximization (EM) algorithm is generally utilized. We define the latent variable r_k that is 1 if data $\boldsymbol{x}_i (i = 1, \cdots, N)$ belongs to the k-th distribution; otherwise, 0. The following procedures are the EM algorithm.

E-step

The cloud server calculates the posterior distribution of r_k as follows:

$$e_k^{(t)}(\boldsymbol{x}_i) = \frac{\alpha_k^{(t)} g_k(\boldsymbol{x}_i|\boldsymbol{\theta}_k^{(t-1)})}{\sum_{j=0}^{K-1} \alpha_j^{(t)} g_j(\boldsymbol{x}_i|\boldsymbol{\theta}_j^{(t-1)})}, \tag{11}$$

where $e_k^{(t)}(\boldsymbol{x}_i)$ denotes the posterior distribution of r_k and t is the iteration index.

M-step

Each parameter is updated as follows:

$$\alpha_k^{(t)} = \frac{1}{N} \sum_{i=1}^{N} e_k^{(t)}(\boldsymbol{x}_i), \tag{12}$$

$$\boldsymbol{c}_k^{(t)} = \frac{\sum_{i=1}^{N} e_k^{(t)}(\boldsymbol{x}_i) \boldsymbol{x}_i}{\sum_{i=1}^{N} e_k^{(t)}(\boldsymbol{x}_i)}, \tag{13}$$

$$\boldsymbol{\Sigma}_k^{(t)} = \frac{\sum_{i=1}^{N} e_k^{(t)}(\boldsymbol{x}_i)(\boldsymbol{x}_i - \boldsymbol{c}_k^{(t)})(\boldsymbol{x}_i - \boldsymbol{c}_k^{(t)})^{\mathrm{T}}}{\sum_{i=1}^{N} e_k^{(t)}(\boldsymbol{x}_i)}. \tag{14}$$

The cloud server repeats the above steps until the following function O converges:

$$O = \sum_{i=1}^{N} \sum_{j=0}^{K-1} e_j^{(t)}(\boldsymbol{x}_i) \log \alpha_j^{(t)} g_j(\boldsymbol{x}_i|\boldsymbol{\theta}_j^{(t)}). \tag{15}$$

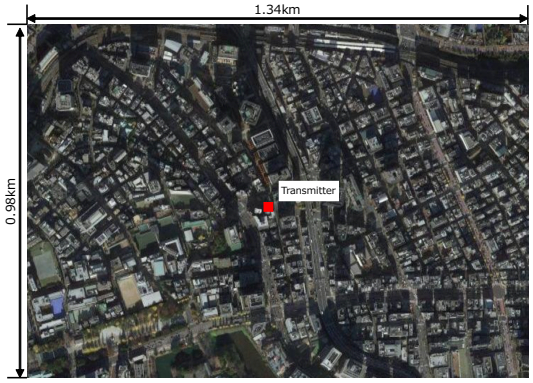

Fig. 2. Measurement environment.

TABLE I
MEASUREMENT SPECIFICATIONS

Transmission power [dBm]	29
Center frequency [GHz]	3.5
Antenna	Ominidirectional
Antenna height of transmitter [m]	17.5
Antenna height of receiver [m]	1.5
Spectrum analyzer	Anritsu MS2712E
Resolution bandwidth [Hz]	300
Walking speed [km/h]	4
Measurement interval [ms]	0.15

VI. 3.5GHz Band Datasets

To evaluate the validity of the shadowing classification, this paper uses the measured data over 3.5GHz band [10]. The experiment campaign was conducted in Kudanshita Chiyoda-ku in Tokyo, Japan. There are many buildings in the area; thus, the environment is an urban. Fig. 2 presents the experiment environment and the red square denotes the location of the transmitter. The transmitter sent the continuous wave to each location. Meanwhile, the receiver having the spectrum analyzer recorded the instantaneous received signal power and reception location while walking at about 4 [km/h]. Table I shows the experiment parameters. We used 100423 samples to construct the shadowing classifier.

VII. Emulation Results

This section mentions the evaluation results. The comparative methods use the weights of 0.1 and 0.9 for (x_l, y_l) and s_l, respectively.

A. Example of Radio Maps

Fig. 3 indicates the examples of the radio map and shadowing classification. Fig. 3(a) is the true radio map that visualizes the average received signal power in each 10m mesh. Meanwhile, the others are the classified shadowing maps. Here, D is 4 and K is 218 that corresponds to $w = 0.2$ [dB]. These maps clarify that the shadowing realizations can be appropriately classified. For example, around the southeast area in Fig. 3(a), the average received signal power is similar; that is, the spatial correlation of the shadowing can be found. Each shadowing map reveals that similar shadowing realizations can be classified in the area.

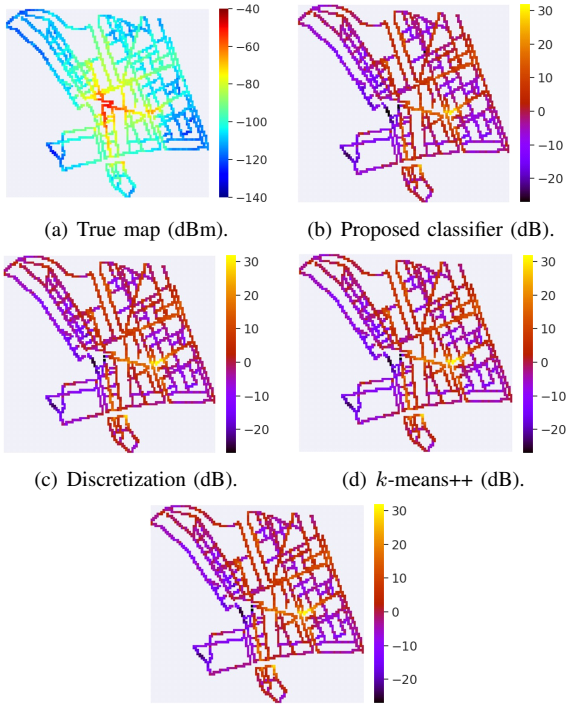

(a) True map (dBm). (b) Proposed classifier (dB).

(c) Discretization (dB). (d) k-means++ (dB).

(e) GMM (dB).

Fig. 3. Examples of the radio map and shadowing classification.

B. Estimation Accuracy

This subsection evaluates the prediction accuracy of each method using RMSE as follows:

$$\mathrm{RMSE} = \sqrt{\frac{1}{L_{\mathrm{eva}}} \sum_{i=1}^{L_{\mathrm{eva}}} (p_i - \bar{p}_{i,\mathrm{predcted}})^2} \quad [\mathrm{dB}], \tag{16}$$

where p_i [dBm] is defined as an instantaneous received signal power in the i-th mesh. $\bar{p}_{i,\mathrm{predcted}}$ [dBm] denotes the estimated power in the i-th mesh, and L_{eva} is the number of 10m meshes. We divided 100423 samples into 3 groups and performed the cross-validation.

The prediction accuracy is depicted in Fig. 4. The RMSE of the Radio map is calculated using the median received signal power in each mesh without the shadowing classification. Meanwhile, the Fitted path loss estimates the average received signal power based on the path loss parameters b and a. Note that D is 0 in the Discretization; thus, a shadowing realization is stored as an integer value in each mesh. These numerical values mean that the average RMSE becomes small in the proposed classifier, k-means++, and GMM as K increases. The Discretization-based method can skillfully calculate the average received signal power; however, the accuracy saturates around 4.2 [dB] owing to the discretization error. In contrast, the proposed classifier can slightly improve the RMSE because

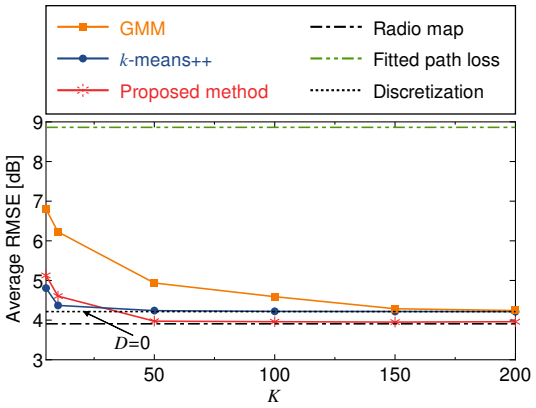

Fig. 4. Estimation accuracy.

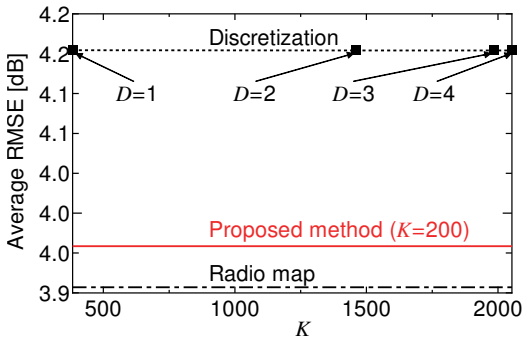

Fig. 5. Average RMSE of the proposed classifier and discretization.

TABLE II
ACCUMULATION ITEMS IN CLASSIFIER AND COMPARISON METHODS

(a) Mesh Table

Element	Type	Size [byte]
Mesh code (10m)	text	11
Shadowing label (Cluster label) k	int	4
Total data size per mesh		15

(b) Shadowing Table

Element	Type	Size [byte]
Shadowing label (Cluster label) k	int	4
Shadowing realization $\hat{s}_k$	double	8
Total data size per model		12

(c) Single Table

Element	Type	Size [byte]
b, a	double	16
Transmitter mesh code	text	16
1st mesh code	text	5
Total data size		37

TABLE III
ACCUMULATION ITEMS IN THE RADIO MAP

(a) Mesh Table

Element	Type	Size [byte]
Mesh code (10m)	text	11
Average received signal power	double	8
Total data size per mesh		19

(b) Single Table

Element	Type	Size [byte]
1st mesh code	text	5

the shadowing realization is classified by considering the small-scale fading.

Additionally, the RMSE between the classifier and discretization is shown in Fig. 5. In the Discretization-based method, the four plots indicate the accuracy using $D = 1, 2, 3, 4$, respectively; thus, there are many shadowing models in large D. Note that the RMSE of the proposed classifier is calculated in $K = 200$ that corresponds to the right end in Fig. 4. These values show that the RMSE is not improved in the Discretization-based method even if D increases. Meanwhile, the proposed classifier is superior to the Discretization-based method with small K. From the results, we argue that the Discretization-based method should not be used in D is 1 or more because the registered data size unnecessarily increases.

C. The Registered Data Size

Finally, this subsection calculates the data size to verify the effectiveness of the shadowing classification. Tables II and III present the accumulation items of the proposed classifier and conventional radio map, respectively. The proposed classifier and comparative methods construct K shadowing models; thus, a shadowing value is managed with the label k in the shadowing table as shown in Table II(b). These elements are registered for K models. To reduce the accumulated data size, mesh table as defined in Table II(a) stores the label k as the integer in each mesh. Although the reference [7] presents the 10m mesh code as text type with 16 [byte], this paper considers the size as 11 [byte] by considering the constant value of the 1st mesh code. The remaining size of 5 [byte] is accumulated in Table II(c) with b, a, and the transmitter mesh code.

Meanwhile, Table III(a) shows the accumulation items in the conventional radio map. The table registers the average power value with 10m mesh code. The 1st mesh code is registered in Table III(b).

In the shadowing discretization with $D = 0$, the shadowing realization is accumulated as the integer; thus, Table II(a) is used with the discretized shadowing value instead of the label k. Meanwhile, in D is 1 or more, since the discretized shadowing value is created as the floating point type, Tables II(a) and II(b) are used. In both cases, Table II(c) is utilized to calculate the path loss.

In summary, the total data size of the proposed classifier and comparative methods can be expressed as follows:

$$A_1 = (L \times 15) + (K \times 12) + 37 \quad [\text{byte}], \tag{17}$$

where A_1 is the accumulated data size in the proposed classifier and comparative methods. Additionally, the accumulated

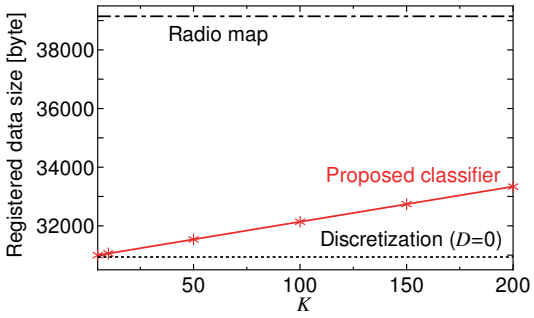

Fig. 6. The accumulated data size.

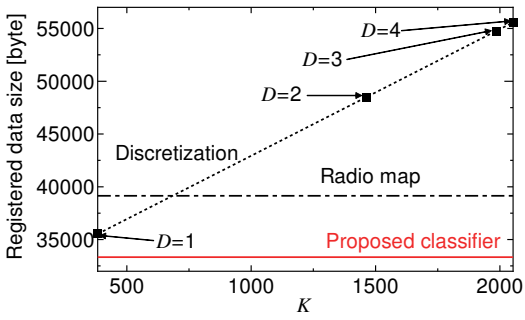

Fig. 7. The registered data size of the proposed classifier and quantization.

data size of the conventional radio map A_2 can be defined as,

$$A_2 = L \times 19 + 5 \quad [\text{byte}]. \tag{18}$$

Finally, the data size of the discretization with $D = 0$ is given by

$$A_3 = L \times 15 + 37 \quad [\text{byte}], \tag{19}$$

where A_3 is the registered data size of the discretization-based method. Note that $A_3 = A_1$ in D is 1 or more.

Fig. 6 depicts the data size in each method with $L = 2060$. This figure clarifies that the proposed classifier and discretization-based method can decrease the data size around 14.8–20.8 [%] compared to the conventional radio map. If the slight degradation of the RMSE is tolerated, the discretization-based method with $D = 0$ may be useful in terms of the registered data size. If not, the proposed classifier should be utilized.

The registered data size of the discretization as D is 1 or more is illustrated in Fig. 7. It can be confirmed that the data size increases in an increase of D. Additionally, since the number of same shadowing realizations is little, the size becomes large compared to the conventional radio map. Thus, in the discretization, the shadowing realization should not be accumulated with floating point type.

VIII. Conclusion

This paper has evaluates the shadowing classification toward to the low storage radio map. As the reduction of the data size, we have considered three methods: the shadowing classifier, the discretization-based method, and conventional clustering algorithms. The performance evaluation has revealed that the proposed classifier is suitable in terms of the prediction accuracy and data size. Additionally, the discretization-based method with $D = 0$ is useful if the slight degradation is tolerated.

Acknowledgment

This work was supported by JSPS KAKENHI Grant Numbers 18H01439, 18KK0109, 19J23352.

References

[1] S. H. Jung and D. Han, "Automated construction and maintenance of Wi-Fi radio maps for crowdsourcing-based indoor positioning systems," *IEEE Access*, vol. 6, pp. 1764–1777, Dec. 2017.

[2] X. Ying, S. Roy, and R. Poovendran, "Pricing mechanism for quality-based radio mapping via crowdsourcing," in *Proc. 2016 IEEE GLOBECOM*, Washington, DC, USA, Dec. 2016, pp. 1–6.

[3] M. Gudmundson, "Correlation model for shadow fading in mobile radio systems," *Electron Lett.*, vol. 27, no. 23, pp. 2145–2146, Nov. 1991.

[4] K. Katagiri, K. Sato, K. Inage, and T. Fujii, "Experimental verification of shadowing classification for radio map," in *Proc. 92nd IEEE VTC2020-Fall*, Victoria, BC, Canada, Dec. 2020, pp. 1–7.

[5] X. Wang, M. Umehira, B. Han, P. Li, Y. Gu, and C. Wu, "Online incentive mechanism for crowdsourced radio environment map construction," in *Proc. IEEE ICC 2019*, Shanghai, China, May 2019, pp. 1–6.

[6] Y. Ye and B. Wang, "Rmapcs: Radio map construction from crowdsourced samples for indoor localization," *IEEE Access*, vol. 6, pp. 24224–24238, Apr. 2018.

[7] K. Sato, M. Kitamura, K. Inage, and T. Fujii, "Measurement-based spectrum database for flexible spectrum management," *IEICE Trans. Commun.*, vol. E98-B, no. 10, pp. 2004–2013, Oct. 2015.

[8] Y. Uesugi, K. Katagiri, K. Sato, K. Inage, and T. Fujii, "Clustering for signal power distribution toward low storage crowdsourced spectrum database," *IEICE Trans. Commun.*, vol. E104-B, no. 10, pp. 1237–1248, Oct. 2021.

[9] R. Hasegawa, K. Katagiri, K. Sato, and T. Fujii, "Low storage, but highly accurate measurement-based spectrum database via mesh clustering," *IEICE Trans. Commun.*, vol. E101-B, no. 10, pp. 2152–2161, Oct. 2018.

[10] K. Katagiri, K. Onose, K. Sato, K. Inage, and T. Fujii, "Highly accurate prediction of radio propagation using model classifier," in *IEEE 89th VTC2019-Spring*, Kuala Lumpur, Malaysia, Apr. 2019, pp. 1–5.